Analysis of Process Parameter Effects on Forming Quality in Micro Single Point Incremental Forming (μSPIF)

Mohamed Nizam Bin Mohamed Ismail[1], Darren Low Wei Wen[1], Ganesh Kumar Meenashisundaram[1], Kai Soon Fong[2], and A. Senthil Kumar[1]*

[1]Department of Mechanical Engineering, National University of Singapore, 9 Engineering Drive 1, Block EA, Singapore 117576, Singapore

[2]Singapore Institute of Manufacturing Technology (SIMTech), Agency for Science, Technology and Research (A*STAR), 5 CleanTech Loop #01-01, CleanTech Two Block B, Singapore 636732, Republic of Singapore

*Corresponding Author asenthil@nus.edu.sg (A. Senthil Kumar)

Abstract

Micro Single Point Incremental Forming ($\mu SPIF$), the process of shaping parts with at least two dimensions smaller than 1 mm, is a promising microfabrication technique known for its near-net-shape capability and high productivity. The growing trend of miniaturization across various industries has led to increased demand for microproducts and microdevices. The influence of forming parameters is critical for improving metal formability, as well as enhancing geometrical accuracy and productivity. Accordingly, this paper aims to examine the influence of forming parameters, such as spindle speed and feed rate, on mean forming forces, force deviations, and their subsequent effects on the formability of 304 stainless steel parts fabricated using single-point incremental forming.

Experiments were conducted using 304 stainless steel foil of $50\mu m$ thickness, formed with slender forming tools featuring ball-nose tips of 3 mm and 1 mm diameters, both with a tool height of 12.5 mm. Frustum pyramids were formed with edge radii of $500\mu m$ and step-down of $100\mu m$, with varying spindle rotation and feed speeds. The analysis was done quantitatively using force and geometric data, along with a qualitative study of the formed surfaces. This systematic approach helped identify the optimal parameters for slender tool applications in $\mu SPIF$. The optimal parameters determined were a tool speed of 6000 rpm and a feed rate of 750 mm/min. The results were experimentally verified through successful forming of of a two-shaped structure geometry comprising a hybrid pyramid and cone geometry using the identified tool speed and feed rate.

Keywords: Microforming, single-point incremental forming, forming parameters, forming force, 304 stainless steel, hybrid forming.

1. Introduction

Metal forming is a widely used manufacturing technique in industries such as automotive, aerospace, and home appliances. It involves shaping metallic materials, like sheets, by applying force to alter their structure and achieve a desired design [1]. Traditional sheet metal forming processes often face challenges, including high costs due to specialized dies and limitations in producing complex shapes. As a result, incremental sheet forming (ISF) has emerged as a promising alternative in sheet metal processing [2].

ISF is a flexible, die-less technique where a sheet metal blank is secured by two retaining rings and shaped by a hemispherical punch that follows a programmed toolpath. The process is carried out incrementally [3]. ISF can be classified into two main types: single-point incremental forming (SPIF) and double-sided incremental forming (DSIF) [4]. The former employs the use of a single forming tool whereas the latter utilizes two forming tools (one on each side of the workpiece). Among these, SPIF is the most widely adopted due to its simpler setup and ability to produce high-quality results with minimal defects, provided the operating parameters are carefully controlled [4, 5].

Micro Single Point Incremental Forming ($\mu SPIF$) is a specialized subset of SPIF, primarily used for producing thin metal components in industries such as aerospace, biomedical, automotive, home appliances, marine, and prototyping. In this process, a hemispherical tool incrementally shapes the metal sheet, similar to conventional SPIF, but both the tool and sheet metal thickness are reduced to micro-scale dimensions [6]. The shift to micron scales introduces significant size-effects that influence the material's [6] and tool behaviour during the forming process [5].

Precise evaluation of operating parameters is crucial in $\mu SPIF$. Spindle speed, feed rate and step-down height influence forming speed, which refers to the relative motion between the tool and the metal sheet. This is a critical factor in metal forming processes, as friction generated during motion produces heat [7]. The heat is directly proportional to forming speed, and higher speeds can lead to poor surface roughness, accelerated tool wear, and breakdown of the lubricant film. Managing the forming speed is crucial to balance productivity with part quality [2].

Increased tool radius, sheet thickness, or step-down height results in higher forming forces. Additionally, materials with greater yield strength require more force for deformation. The heat generated from friction can reduce the force needed for deformation, improving process efficiency [8]. Tools with smaller radii offer better formability due to the reduced contact area during forming. In contrast, larger radius tools increase the contact area with the metal sheet, resulting in higher forming forces. However, smaller radius tools concentrate deformation into a more localized area, generating higher strain and improving formability [9].

Previously, Ankush Bansal et al. [10] analysed the forming forces, geometric accuracy, and material formability of 50 μm thick AL 1100-O and AL 5052-H19 foils. The forming forces in incremental forming were found to be similar for both macro-scale and micro-scale parts; however, the axial force fluctuation in micro-scale parts was significantly higher at 13%, likely due to the planar anisotropy of the AL 5052-H19 material. Cross-sectional profiles of conical and funnel-shaped parts were compared with their designed geometries, revealing geometric deviations of 90–100 μm caused by sheet spring-back and tool deflection during fabrication. The material formability of AL 5052-H19 foil was evaluated, with a maximum wall angle of 41.8° achieved before fracture, lower than in macro-scale ISF but higher than in tensile test results. Additionally, a unique feature twist defect was observed in pyramid-shaped parts, attributed to increased step size and tool deflection, which could be mitigated by improving tool rigidity or optimizing the toolpath planning strategy. Thirumalai Muthusamy et al. [11] highlighted that vertical step-down has the most significant influence on the quality of miniature components in $\mu SPIF$, followed by spindle speed, feed rate, and tool tip diameter. Stainless steel foils of 0.04 mm thickness and hemispherical end tool tip diameters of 200 μm and 300 μm were used for the forming experiments. The optimal parameters identified include a 200 μm tool tip, a spindle speed of 2500 rpm, a vertical step-down of 30 μm, and a feed rate of 20 mm/min. Increasing spindle speed was found to reduce forming forces, likely due to hydrodynamic lubrication between the tool and foil, indicating the advantages of higher rotational speeds. Furthermore, it was observed that the forming forces in the Z-direction generally increased with incremental forming depth. The ability of $\mu SPIF$ to reliably produce micro-scale geometries demonstrates sufficient process adequacy for fabricating micro-components.

Stainless steel 304 is frequently selected for forming processes due to its austenitic structure, which offers high ductility and toughness, making it ideal for complex and intricate shaping. Its excellent formability allows it to undergo significant deformation without compromising structural integrity, a key requirement in micro-forming applications that involve high strain. Additionally, its widespread industrial use and resistance to corrosion and various chemicals ensure material reliability and consistency, making it an excellent choice for micro-forming experiments [12].

While existing research provides valuable insights into the mechanics and material behaviour of $\mu SPIF$, there remains a noticeable gap in studies focusing on the optimization of process parameters for enhanced geometric accuracy, formability, and defect mitigation. The limited literature on $\mu SPIF$, especially regarding its applications to specific materials like stainless steel 304, underscores the need for further investigation.

To bridge these gaps, this study will investigate the influence of key process parameters on $\mu SPIF$ (Micro Single Point Incremental Forming) performance, focusing on their effects on forming forces, surface roughness, and defect formation. The paper will commence by introducing the materials used, the forming setup, and data acquisition methods. Following this, the experimental section will detail the impact of spindle speed (3.1.1) and tool diameter (3.1.2). In section 3.1.3, a comprehensive experiment examines the effects of various combinations of spindle speed and feed rate. The results are summarized in Section 3.2, with validation on new geometries presented in Section 3.3. The paper concludes with a summary of the findings in Section 4.

2. Material and Methods

2.1. Materials

The sheet metal used in this paper consisted of 40x40mm AISI 304 stainless steel. The chemical composition of the AISI 304 stainless steel is shown in **Table 1**.

The forming experiments were conducted using slender forming tools made of hardened tool steel with ball-nose tips of 3 mm and 1 mm diameters, respectively. Both tools were mounted on the spindle with an exposed tool height of 12.5 mm. The selection of these specific tool dimensions was aimed at exploring the effects of tool size on the forming process and the resultant part geometry. The 3 mm diameter tool, being larger, was chosen to establish baseline performance metrics and to investigate the forming process under conditions more typical of conventional incremental sheet forming. In contrast, the 1 mm diameter tool was selected to probe the limits of micro-forming capabilities, enabling the fabrication of more intricate features and potentially revealing size-effects that become more pronounced at smaller scales.

Table 1 *Chemical Composition (wt.%).*

C	**Mn**	**F**	**S**	**Si**	**Cr**	**Ni**	**P**	**Ti**
0.08	2.00	0.045	0.03	1.0	17.0-19.0	9.0-12.0	0.045	0.70 Max

2.2. Methods

2.2.1. μSPIF setup

The $\mu SPIF$ equipment was designed and built in-house at the National University of Singapore, and its setup is shown in **Figure 1**. The equipment setup has been comprehensively detailed in our previous work [13]. A Beckhoff CX2040 PLC, equipped with an Intel i7 quad-core processor, was selected as the controller. The machine stage featured three axes, each powered by Yasakawa SGM7J motors, which were managed by individual Yasakawa SGD7S controllers. Nakanishi EM-3030T-J spindle capable of reaching speeds up to 30,000 RPM, was used. The spindle's speed and performance were controlled by a Nakanishi E3000 unit, interfaced with the PLC through analogue and digital signals. A Kistler 9256C 3-axis dynamometer was mounted on the stage to measure forming forces. While 3-axis force data was collected, this paper will only use forces in Z-axis for force analysis (Fz). Sensor data was collected by a Kistler KiDAQ unit at 100Hz, which communicated with the PLC via EtherCAT.

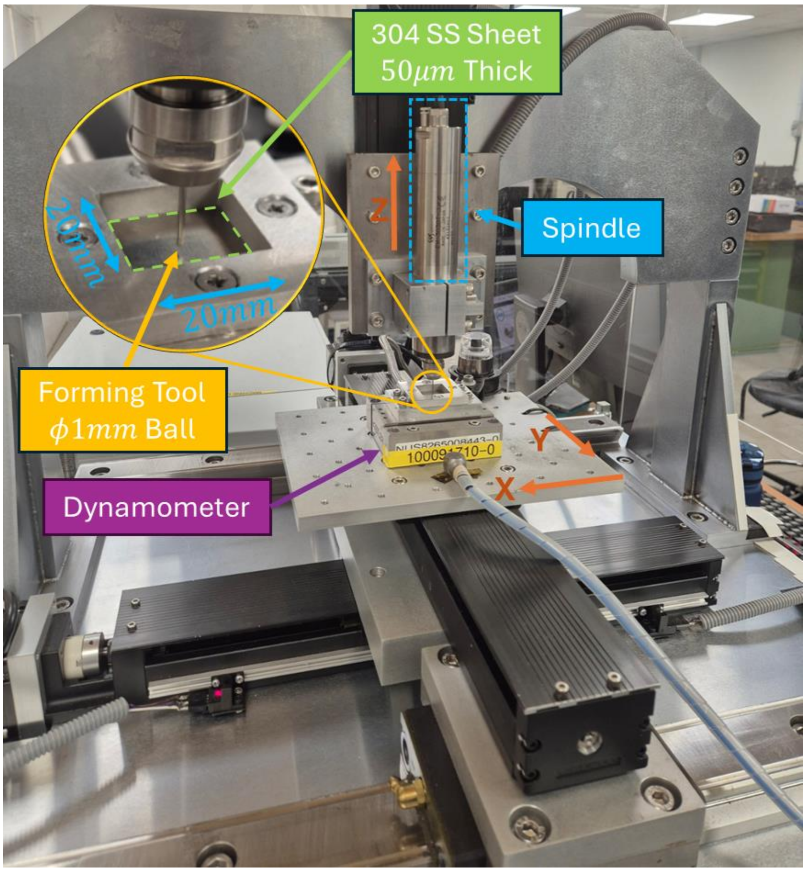

***Figure 1** μSPIF equipment setup*

The selection of geometric shapes for this study, specifically the pyramid and frustum pyramid, is a commonly used geometry in the analysis of Incremental Sheet Forming [14]. The toolpath was generated using SolidWorks CAM, with the tool assumed as a ball-nosed milling tool with an identical diameter for toolpath generation. The specific forming parameters will be presented in section 3.

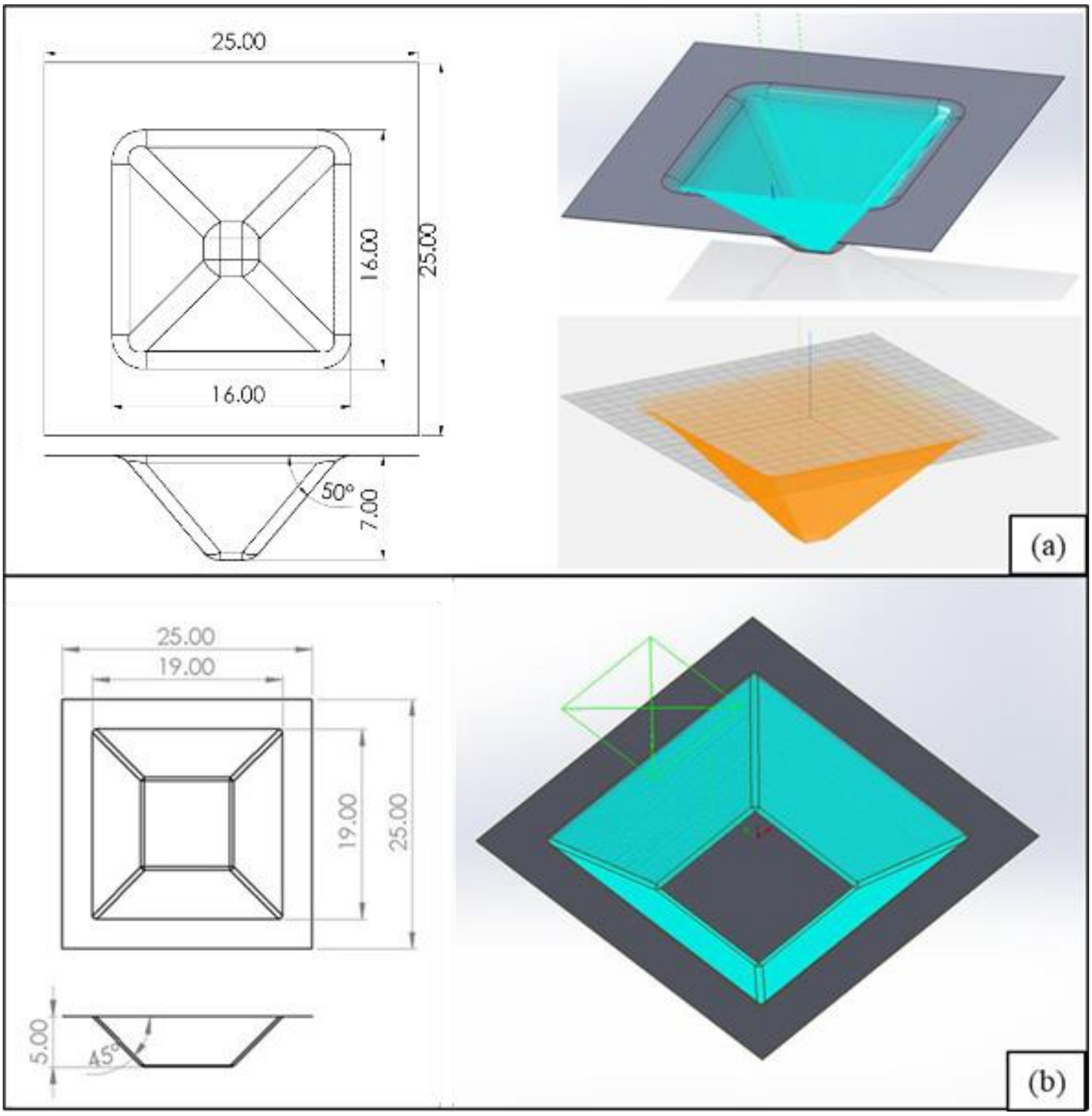

Figure 2 *CAD Drawing and the plotted toolpath for (a) 7mm depth with 1.5mm fillet radius and (b) 5mm depth with 0.5mm fillet radius*

When mounted, the fixture clamps the top and bottom of the sheet, resulting in an exposed forming area of 20x20 mm (**Figure 1**). A 1 and 3 mm diameter ball-nose forming tool was selected for the initial experiment, with the tool rotation set to 0 RPM and 10000 RPM, respectively, at a constant feed rate of

1000 mm/min, as shown in **Table 2**, to study the influence of tool rotational speed and tool radii on the resulting forming forces and geometric outcomes in $\mu SPIF$.

Table 2 *Process parameters for initial preliminary study on tool speed and tool size*

Preliminary Study		
Tool Size	Tool rotation (RPM)	Step-down (μm)
1mm	0	50
	10000	
3mm	0	
	10000	

Subsequently, a parametric study consisting of 20 $\mu SPIF$ experiments was performed using the 1 mm diameter tool to study the influence of spindle speed and feed rate. The selection of spindle speed was based on research conducted by Cheng, Zinan, et al., [15] which concluded that the optimal RPM for $\mu SPIF$ applications is 10000 RPM. The lower limit was established at 2000 RPM based on experiments by Najm, Sherwan Mohammed, et al [16]. Additionally, the tool feed rate was maintained within the range of 250 mm/min to 1,000 mm/min, based on previous findings [16]. The incremental progression of feed rates and RPM was set at uniform intervals of 250 mm/min and 2000 RPM, respectively as shown in **Table 3**.

Table 3 *Process parameters of 20 µSPIF parametric study experiments*

Process Parametric Study						
Feed rate (mm/min)	Tool rotation (RPM)					Step-down (μm)
250	2000	4000	6000	8000	10000	100
500	2000	4000	6000	8000	10000	
750	2000	4000	6000	8000	10000	
1000	2000	4000	6000	8000	10000	

Prior to the forming process, 2–3 mL of lubricant (Shell Tellus S2 MX 32) was applied, once, to the surface of the 304 stainless steel sheet using a dropper, as shown in Figure 3a. The presence of the lubricant on the surface is visible in Figure 3b. To ensure uniform distribution across the sheet, pressurized air was used to spread the lubricant evenly, as illustrated in Figure 3c.

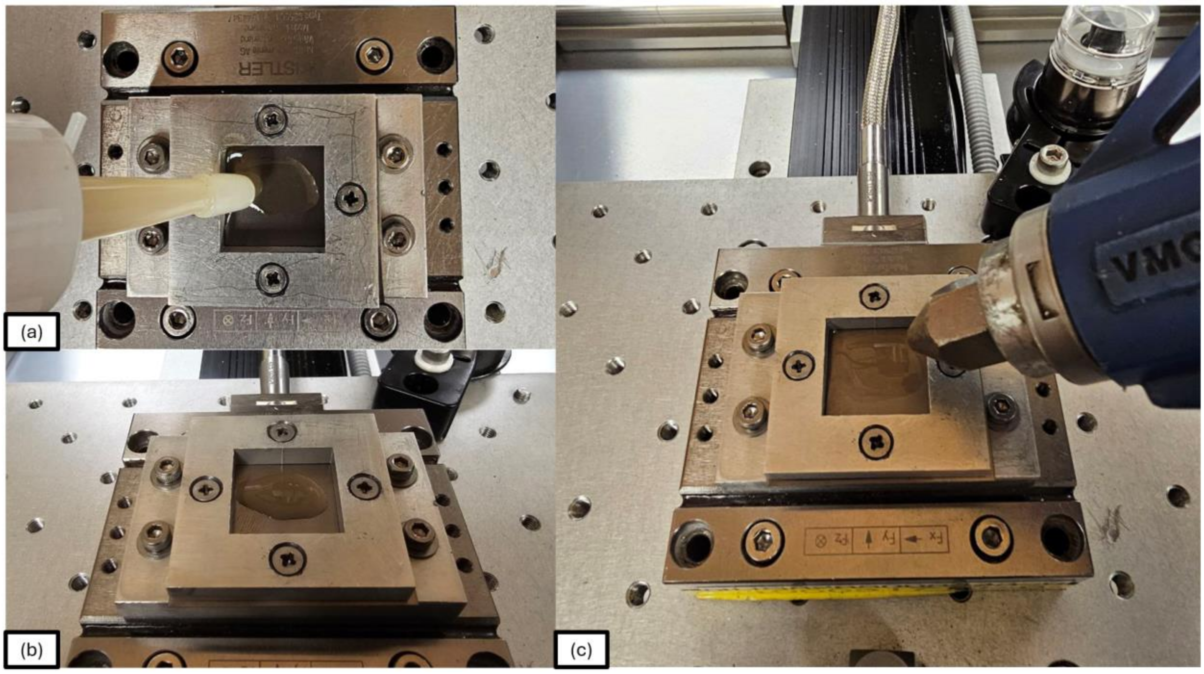

Figure 3 *Lubrication procedure of 304 stainless steel before forming, (a) dropping of lubricant on the surface, (b) lubricant on the surface of the sheet, (c) spreading of lubricant evenly on the surface with the use of pressurized air*

2.2.2. Geometric measurements

Following the forming process, the parts were measured using a portable coordinate measurement machine (CMM) Model 8325 Hexagon Absolute Arm equipped with an RS6 Laser scanner. The use of 3D laser scanning technology allowed for the precise capture of the parts' physical characteristics, enabling detailed digital replication for subsequent geometry analysis and validation. To mitigate the effects of springback that typically occur upon unclamping, the scanning process was conducted while the formed geometries remained secured within the fixture. This non-invasive method ensured accurate measurements without causing deformation of the thin workpieces. The scan data was then saved as an STL file and a comparative analysis was conducted using PolyWorks Metrology software. This comparison facilitated the assessment of discrepancies between the formed parts and the original CAD model.

3. Results and Discussion

3.1. Experimental Results on the formability of 304 stainless steel

3.1.1. Effect of spindle speed on forming forces

Four sets of $\mu SPIF$ experiments were initially conducted. This was done using two separate toolpaths generated using the same geometry (**Figure 2a**), which was used for the 1mm and 3mm diameter forming tools respectively. Both toolpaths were generated using a feed rate of 1000 mm/min with spindle speeds of 0 (free tool rotation) and 10,000 RPM. SolidWorks CAM was used to generate the toolpaths, where a single direction, clockwise, constant Z-Level toolpath strategy was adopted at a step-down of $50\mu m$. This toolpath slices the geometry into planes parallel to the Z axis and generates the toolpath contours for each $50\mu m$. The results for forming force against time are shown in **Figure 4**. The forming time is slightly longer for the 1mm tool as it must traverse slightly longer distances across the target geometry. It was found that the mean forming force decreases significantly with spindle rotation of 10,000 RPM, exhibiting a 39% and 53% reduction for 1mm and 3mm respectively. Additionally, the forming force was approximately 25-60% higher when using a bigger diameter forming tool depending on spindle speed.

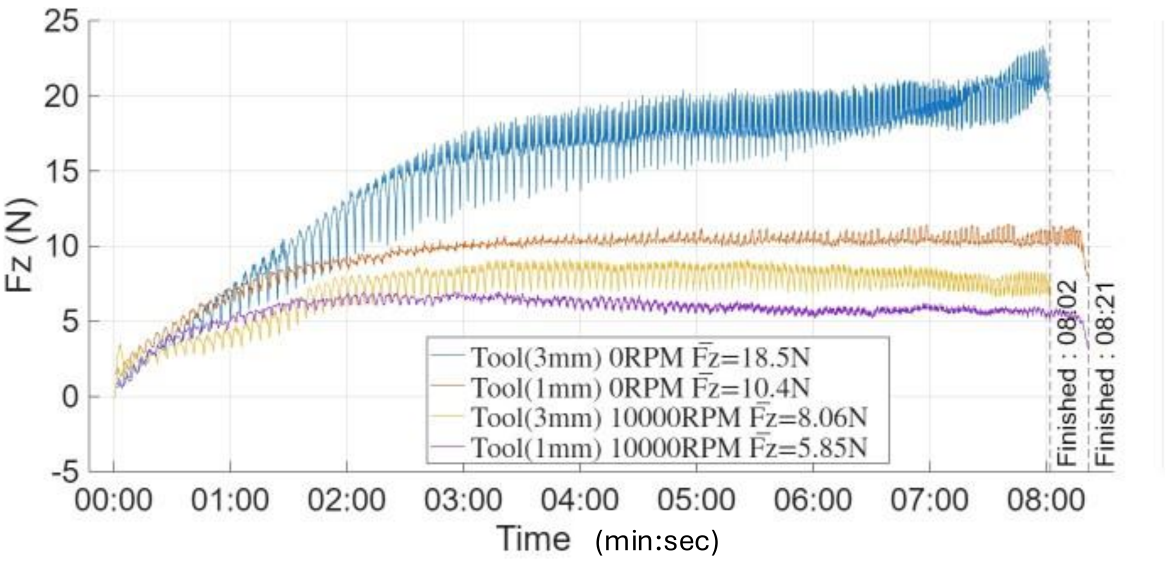

***Figure 4** Forming force against time for varying tool diameters and spindle speed. Moving mean (1 second window) was applied to forming force to improve readability. Mean forming force, $\overline{Fz}$ was obtained using data between 2.5 and 7mm in forming depth.*

During the experiments, an important mechanical phenomenon was observed with the 1mm diameter forming tool. Due to its slender geometry (high length-to-diameter ratio), the tool experienced cyclic bending and straightening during the forming process. This behaviour can be attributed to the combination of forming forces and the tool's relatively low lateral stiffness [17]. The cyclic deformation was particularly noticeable when examining the force measurements, where periodic variations in the forming force correlate with the tool's deflection pattern, as evidenced by the MAD analysis in later sections (3.2.2). This mechanical response helps explain the observed differences in forming behaviour between the 1mm and 3mm tools, as the more rigid 3mm tool maintained better dimensional stability during forming [17]. The tool deflection phenomenon becomes especially relevant when considering the relationship between spindle speed and forming forces, as higher spindle speeds appear to influence the tool's dynamic response and consequently affect both force measurements and surface quality.

3.1.2. Comparison between forming tool diameters

The effect of forming tool diameter was also studied using the previously obtained experimental data. As shown in **Figure 4**, an average forming force reduction of 25-60% was observed with the 1mm diameter tool as opposed to the 3mm diameter tool. This significant force difference can be attributed to the smaller contact area between the tool and workpiece and the mechanical behaviour of the slender 1mm tool [18].

Geometric analysis of the scanned part in **Figure 5** reveals significantly more underforming with the 1mm tool compared to the 3mm tool regardless of spindle speed, which can be partially attributed to the reduced stiffness and subsequent deflection of the smaller diameter tool. A glossier surface finish was also observed at 10,000 RPM for both tool cases when compared to free tool rotation. However, the surface finish for the 1mm tool was noticeably worse than the 3mm tool **(Figure 5)**. The wavy surface produced by the 1mm tool at 10,000 RPM indicates process instability caused by the tool's cyclic deflection behaviour [17]. The more stable surface finish achieved with the 3mm tool can be attributed to its greater rigidity and reduced susceptibility to deflection-induced vibrations.

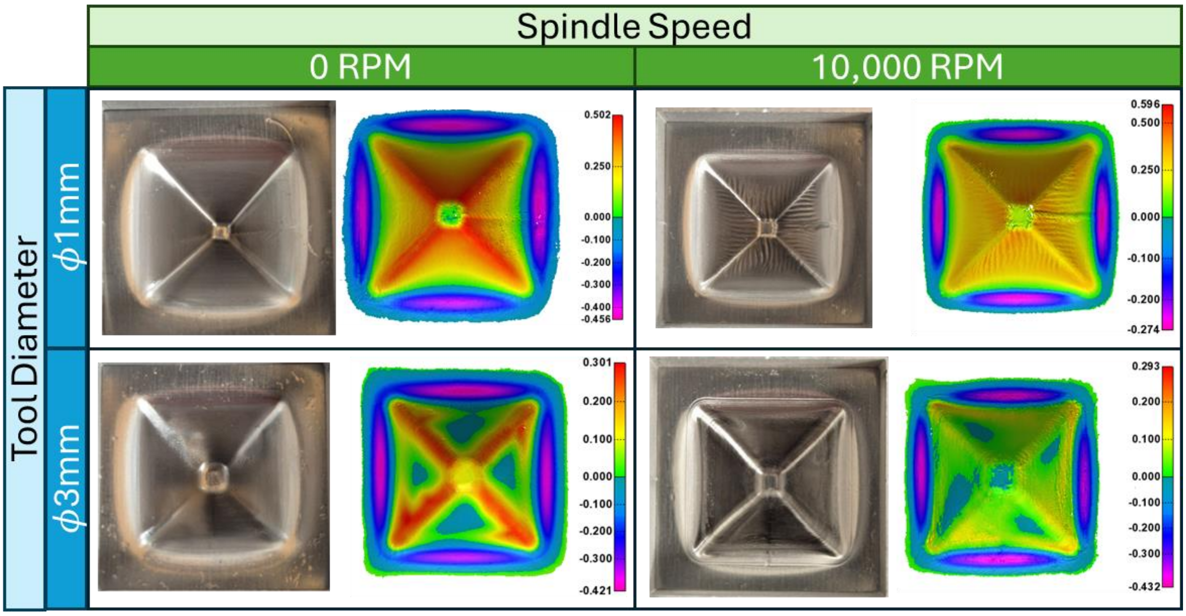

Figure 5 *Forming results with varying spindle speed and tool diameter for the same geometry. Feed of 1000mm/min was used for all four cases. Geometric deviation plot units in mm, positive values indicate underforming.*

Based on this initial forming force analysis and the results from the literature search [15, 16], we further planned our experiments using the 1 mm ball-nose tool to focus the study on improving the formability in $\mu SPIF$ through toolpath generation parameters.

3.1.3. Influence of toolpath parameters on the surface finish of the parts

Using the 1mm diameter ball-nose tool, a total of 20 experiments were planned with the geometry in **Figure 2b**, which has a 0.5 mm fillet radius instead of the 1.5 mm used previously. Furthermore, as fixture-tool clearance for the 3mm tool no longer needs to be considered, the forming area was expanded from 16x16mm to 19x19 mm. To minimise forming time, the toolpath strategy was changed to a continuous spiral with $100\mu m$ step-down. As discussed previously, the spindle speed was varied from 2,000 RPM to 10,000 RPM, and the tool feed rate was adjusted from 250 mm/min to 1,000 mm/min, with incremental progressions of feed rate and RPM set at uniform intervals of 250 mm/min and 2,000 RPM.

Surface defects were quantitatively evaluated by capturing the part geometry using an RS6 laser scanner, which provided a digital point cloud representation of the actual surface. A theoretical, defect-free surface was generated from the scanned model to serve as an ideal reference. Point-to-point measurements between the actual and theoretical surfaces enabled identification of deviation magnitudes across the surface (**Figure 6**). The standard deviation of these measurements provided a statistical measure of surface irregularities (**Figure 7**), with higher deviations indicating poorer surface quality. Based on both the standard deviation values and visual assessment of the formed parts, surface quality could be categorized as: very good (SD < 0.014), good (SD < 0.017), acceptable (SD < 0.018), poor (SD < 0.021), and very poor (SD > 0.021).

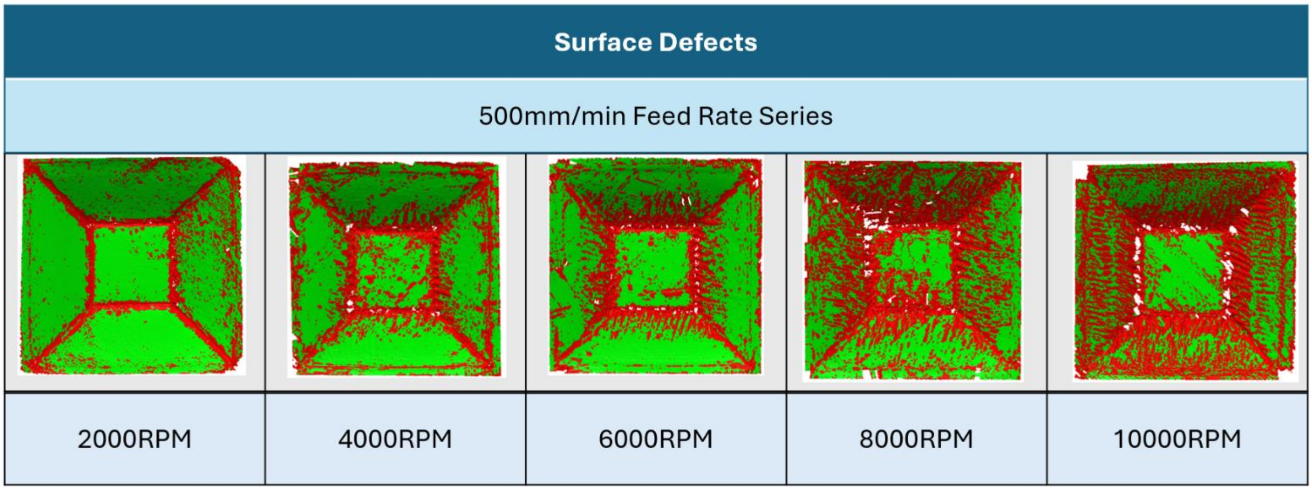

Figure 6 *Surface defect maps for the 500 mm/min feed rate series, formed at spindle speeds from 2000 RPM to 10,000 RPM using the 1 mm diameter tool. The colormap represents the surface deviation for each part, with green indicating deviations within the tolerance limit (≤10 µm) and red indicating regions exceeding the 10 µm surface quality tolerance.*

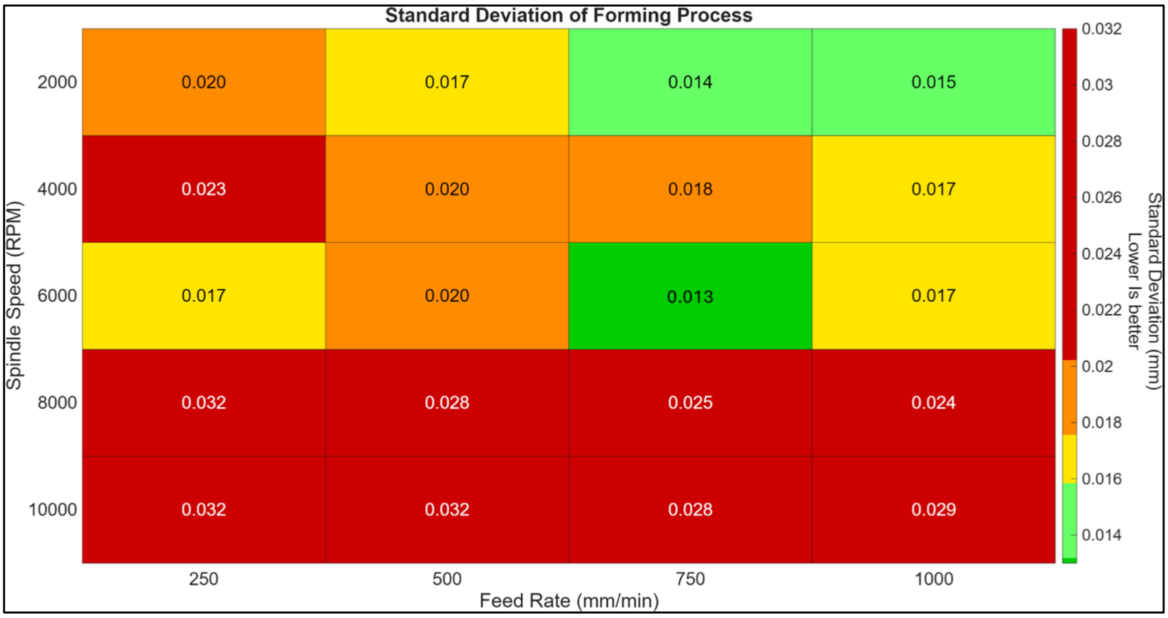

***Figure** 7 Standard deviation of forming process represented based on spindle speed and feed rate, and colour adjusted based on observed surface defects rated qualitatively*

The quantitative results revealed a clear correlation between process parameters and surface quality. The highest deviations occurred at conditions where tool deflection was most pronounced specifically at higher spindle speeds (8,000-10,000 RPM) and lower feed rates (250-500 mm/min). This pattern can be attributed to the observed cyclic bending behaviour of the slender 1mm tool [17], which becomes particularly unstable under these conditions. At higher rotating speeds, the increased frequency of sliding contact leads to greater heat generation at the tool-sheet interface [19]. While moderate heat generation can improve formability through thermal softening, excessive heat at higher speeds (above 6000 RPM) appears to cause process instability, particularly with the slender 1mm tool experiencing cyclic bending.

These quantitative findings were corroborated through visual inspection using a rating scale from 1 to 5, evaluating visible roughness, grooves, wrinkles, jagged edges, and onset length of deformation (**Figure 8**). The visual assessment showed that wrinkled surfaces tend to appear more frequently as spindle rotation speed increases, aligning with the higher standard deviations measured at elevated speeds. Conversely, surface quality improved with increased feed rates, likely due to reduced dwelling time which minimizes both heat generation and the impact of tool deflection at each point.

The optimal forming conditions, 6000 RPM with 750 mm/min feed rate, produced the best results across both quantitative and qualitative assessments, achieving a "very good" surface quality rating with SD < 0.014. This represents conditions where heat generation, friction effects, and tool stability are optimally balanced. The correlation between measured deviations and visual ratings is further supported by the MAD analysis (Section 3.2.2), where increased force variations aligned with poorer surface finishes, suggesting that both metrics effectively capture the impact of tool instability on surface quality.

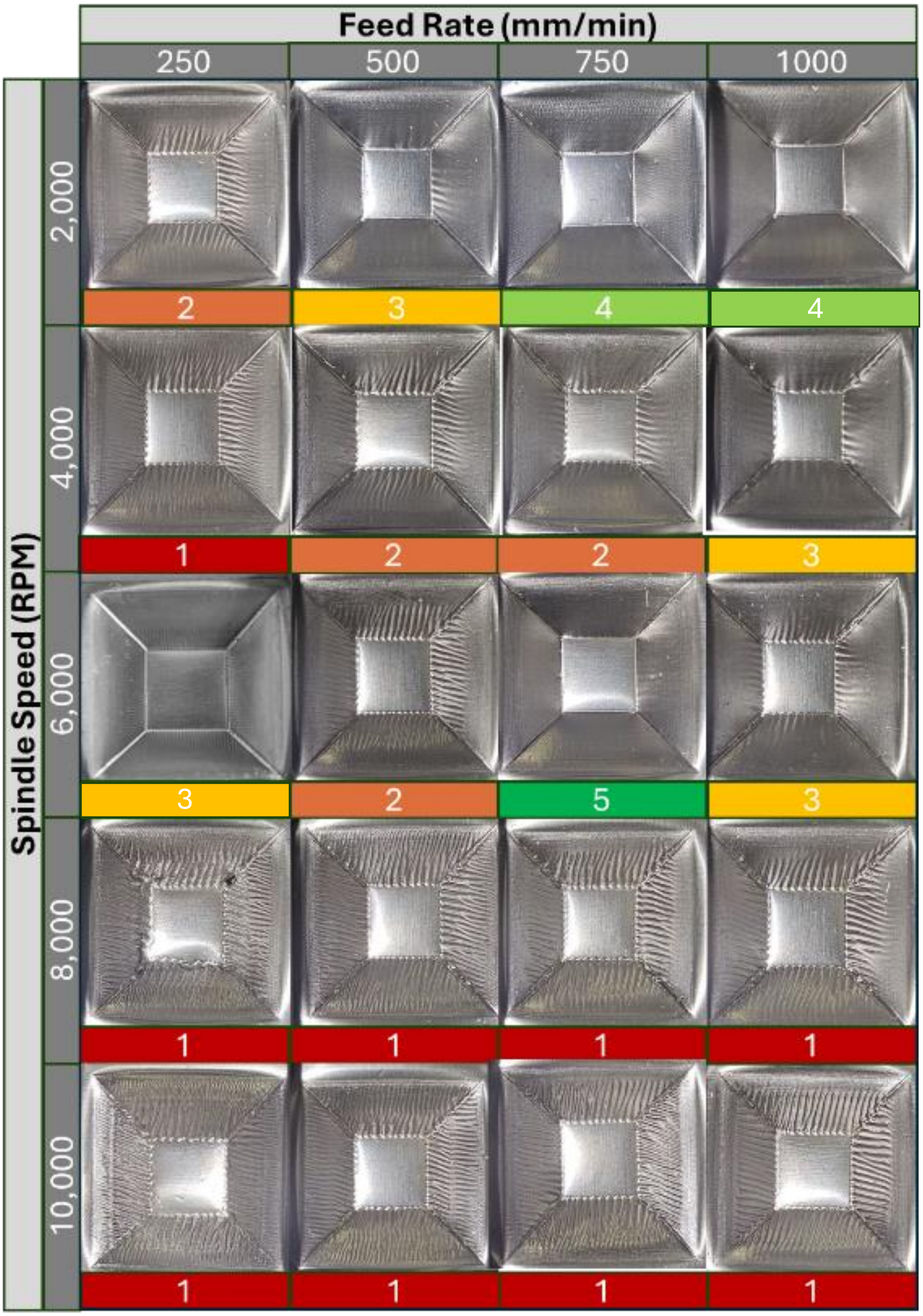

Figure 8 *Post-μSPIF images of parts formed at different spindle speed and feed rates with 1 mm diameter tool. The single digit numbers below the images represent the surface quality based on standard deviation measurements where: very good (SD < 0.014), good (SD < 0.017), acceptable (SD < 0.018), poor (SD < 0.021), and very poor (SD > 0.021). This quantitative assessment aligns with visual observations of surface defects whereby 5 is very good and 1 is very poor..*

3.2. Discussion on forming results

3.2.1. Mean forming force

Figure 9 shows the force in the Z-direction (Fz) plotted against the forming time for the pyramid shape formed with a spindle speed of 2000 RPM. The result shows that as the feed rate increases, the forming time decreases. However, it should be noted that the level of detail in the graphs for feed rates between 500 mm/min and 1000 mm/min is diminished. To overcome this, the x-axis of the force graphs was adjusted to correspond to the depth of the forming tool, ranging from 0 to -5 on the Z-axis (depth) of the CNC machine. The result is reflected in **Figure 10**, where it can be observed that higher feed rates also result in higher forming forces at the same depth (for the same geometry).

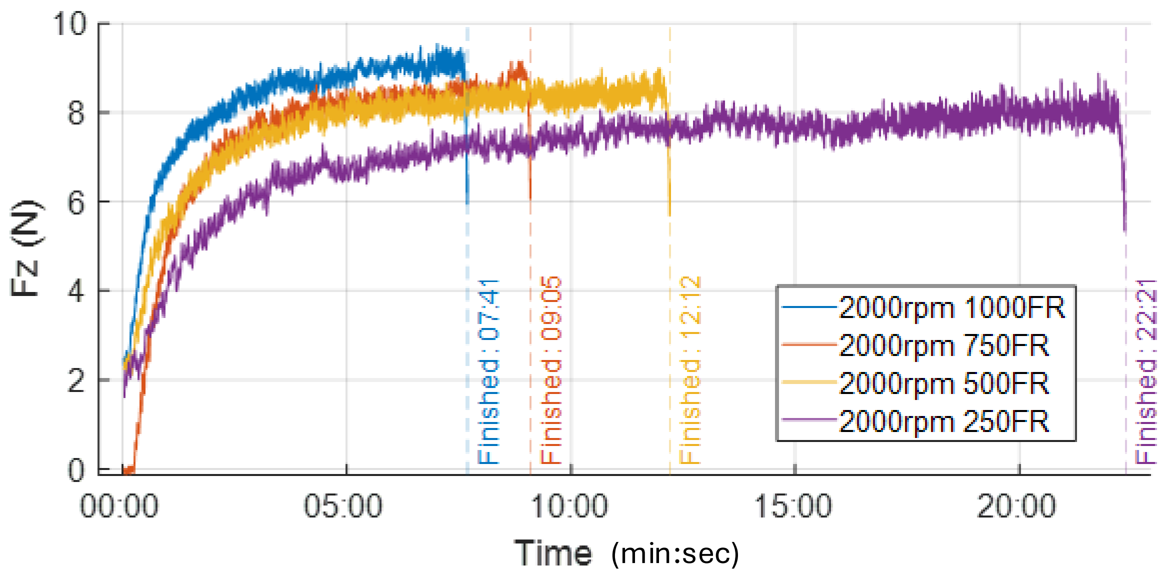

Figure 9 *Forming force (in N) vs time (in min) for 1 mm tool with a rotation speed of 2000 RPM. Moving mean (1 second window) was applied to forming force to improve readability.*

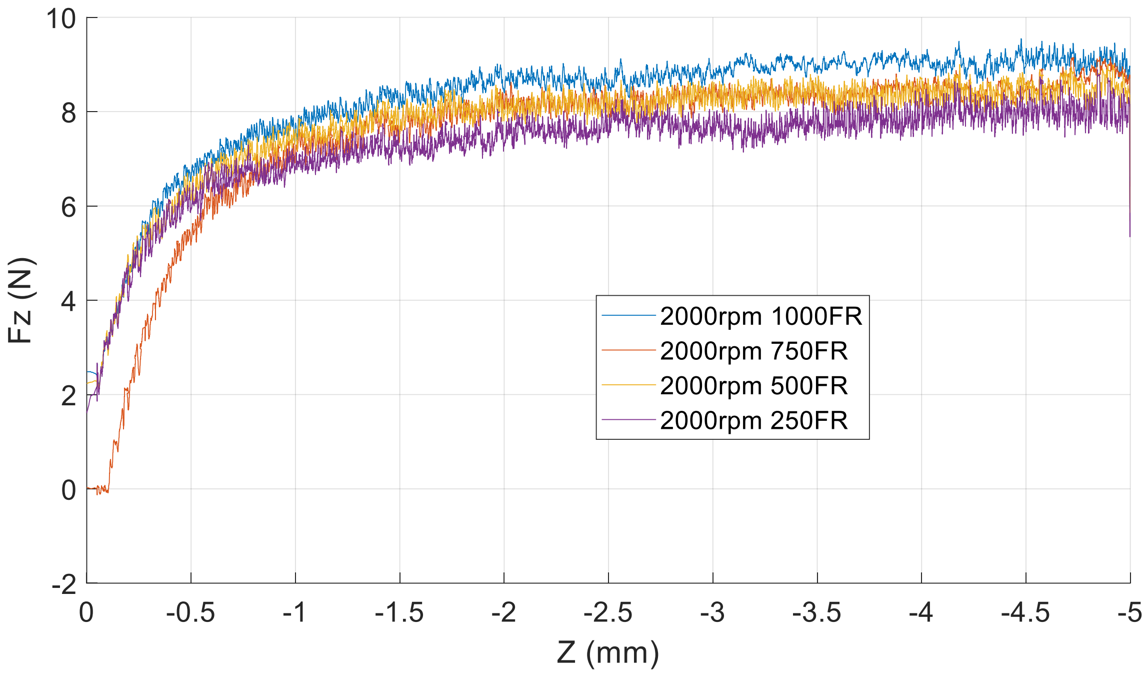

Figure 10 *Forming force (in N) vs depth (in mm) for 1 mm tool with a rotation speed of 2000 RPM. Moving mean (1 second window) was applied to forming force to improve readability.*

To calculate the mean force ($\overline{F_Z}$) per forming parameter combination, the dataset was narrowed down to the forming depth range between -2.5 and -5mm and its $\overline{F_Z}$ was taken. This range was chosen to obtain a more precise measurement of the elevated forming forces for the pyramid geometry. The rationale behind this selection was to also exclude the further variations in tool entry and exit, which were considered outliers and did not reflect the actual forming forces.

With the $\overline{F_z}$ obtained for each forming parameter combination, a polynomial surface plot was generated for comparative analysis as shown in **Figure 11**. This figure reveals a clear trend: as the feed rate increases, the forming force increases, while an increase in spindle speed results in a decrease in forming force. These trends are consistent with the principles of the forming process, where feed rate affects the rate of tool interaction with the material, influencing the forces generated, while spindle speed alters the rate at which pressure is applied to the material [15].

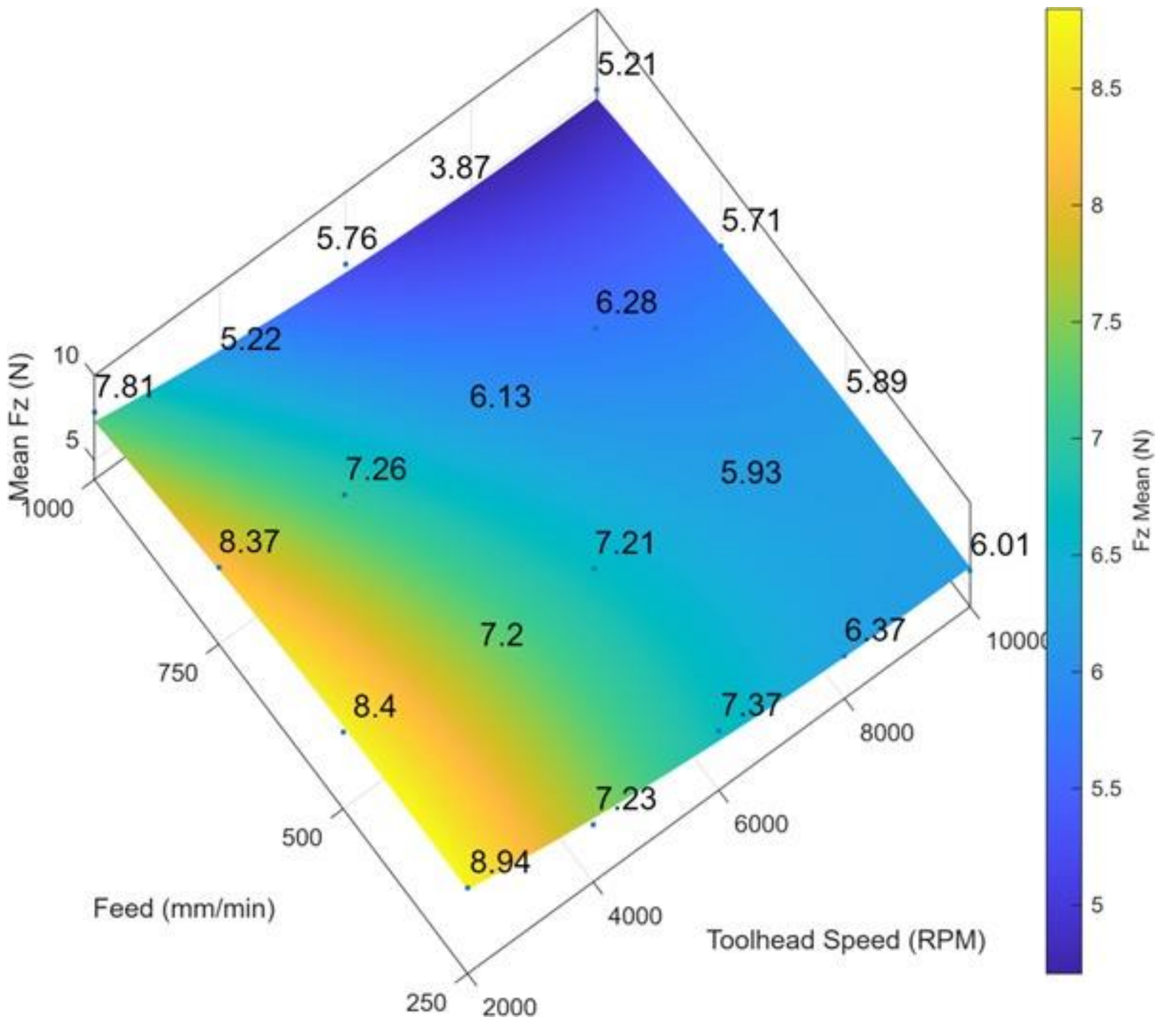

Figure 11 *Mean forming force (Shown in black) at different tool feed rates and spindle speed. The data was fitted as a quadratic polynomial surface and plotted as shown.*

3.2.2. Variation in transient forming force

While the mean forming force can provide a better understanding of the impact of the parameters in $\mu SPIF$, the variation in forming forces can also uncover further information. The variance in mean forming force data points was more pronounced under lower feed rate conditions compared to higher feed rates, which can be attributed to the increased dwelling time allowing the slender tool to experience more pronounced cyclic bending.

To further explore this variability in mean forming force, a data cleaning process was carried out to improve the accuracy and clarity of the force measurements. First, the moving mean (1 second window) was subtracted from the raw data, then the moving Median Absolute Deviation (MAD) was obtained using a sliding window of 1 second. MAD was obtained using **(1)** where A refers to the vector of F_z

with N observations (in the sliding window) for $i = 1,2 \dots N$. The MAD of the forming forces plotted against the tool's depth is illustrated in **Figure 12**. This figure clearly shows that the poor surface finish is highly associated with elevated MAD. The MAD serves as an indicator of the dispersion or variability in the force data, offering insights into the consistency and stability of the forming process under different experimental settings. The cyclic bending of the 1mm tool manifests as periodic force variations, which are captured by the MAD measurements. Also, MAD force values were presented in a bar plot (**Figure 13**) for comparative analysis across the various forming conditions.

$$MAD = median(|A_i - median(A)|) \qquad \textbf{(1)}$$

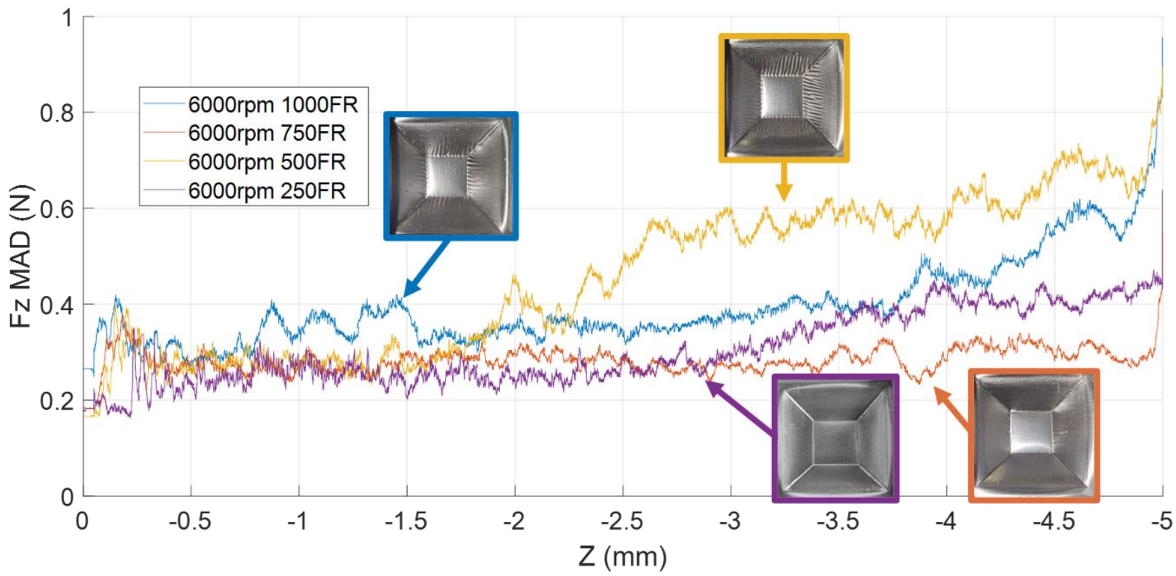

Figure 12 *Force (MAD) vs Depth of pyramid shape parts formed at 6000 RPM. FR denotes feed rate in mm/min.*

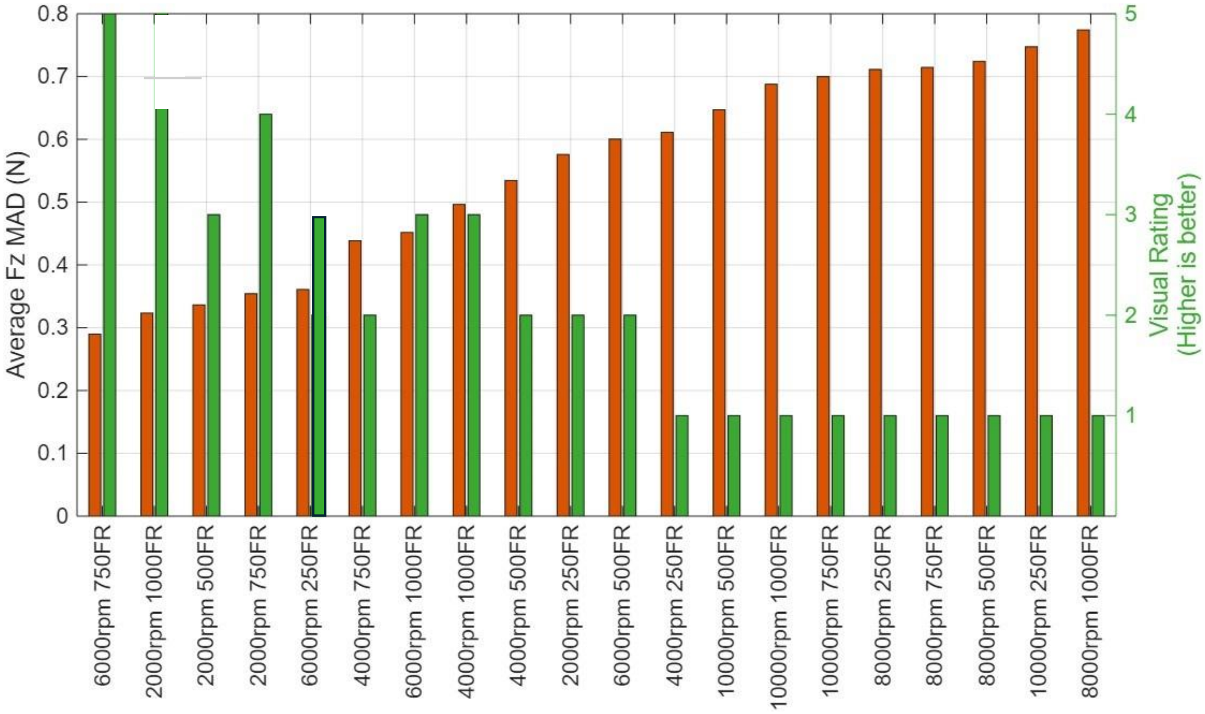

Figure 13 *Bar plot of average MAD below -2.5mm depth (in orange) and visual rating (in green) for different tool feed rates (FR, in mm/min) and spindle speed (RPM).*

An examination of the data in **Figure 12** reveals a clear connection between the force variations and the standard deviation matrix in **Figure 7**, pointing to a link between process parameters and surface quality in $\mu SPIF$. Specifically, the smallest force deviations occurred under two particular conditions: a spindle speed of 6000 RPM combined with a feed rate of 750 mm/min, and a spindle speed of 2000 RPM with a feed rate of 1000 mm/min. These same settings also resulted in the highest surface finish quality, indicating that these parameter combinations achieve optimal tool stability by minimizing the cyclic deflection behaviour. The reduced MAD values under these conditions suggest that the tool maintains more consistent contact with the workpiece, leading to better surface quality and more stable forming conditions.

3.2.3. Geometric deviation

The geometric accuracy of the formed parts was measured using an RS6 Laser Scanner mounted on a Model 8325 Hexagon Absolute Arm**.** During the analysis process, misalignments were found between the scanned geometry and actual CAD geometry. Because the measurement datum differs for both actual and target geometries, manual alignment (positioning) was done to minimise this error. This misalignment in the datum will correspondingly impact the accuracy of geometric deviation measurement.

Using this process, the geometric deviation for the 20 experiments is summarised in **Figure 14**. Notably, this figure shows the wrinkled surface is not only visible (**Figure 8**) but was severe enough to be detected through laser line scanning (**Figure 14**). Since the geometry measurement operates at the edge of its optimal range for such micro-scale parts, inaccuracies in geometric assessment were to be expected, which makes it difficult to make precise conclusions on the geometric deviation.

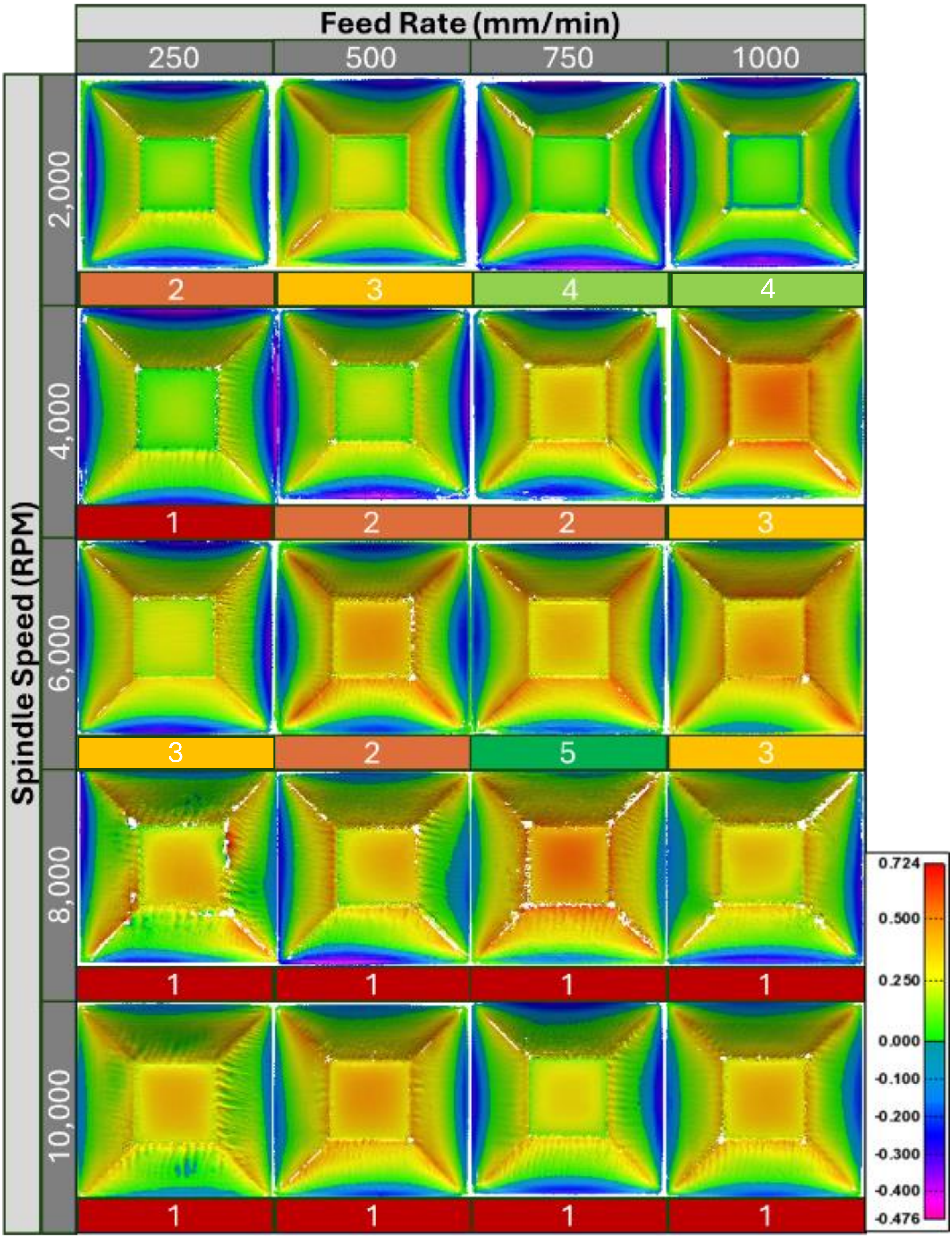

Figure 14 *Post-µSPIF geometric deviation of parts formed at different spindle speed and feed rates with 1 mm diameter tool. The single digit numbers below the images represent the observed surface defects rated quantitatively from 1 to 5, with 5 being the best.*

3.3. Validation experiment through forming of hybrid shapes

The experimental investigations conducted thus far have shown that a spindle speed of 6000 RPM with a feed rate of 750 mm/min produced the most favourable results. To verify that this set of parameters can be applied to various forming geometries, it was compared to a poor-performing parameter set (10000 RPM and 250 mm/min).

Two new validation geometries were introduced in this section, hybrid pyramid and dome (**Figure 15**). The post-forming images and depth maps for the hybrid pyramid and dome are shown in **Figure 16** and **Figure 17** respectively. These results confirm that 6000 RPM and 750mm/min are ideal forming parameters and have been shown to consistently form varying features well.

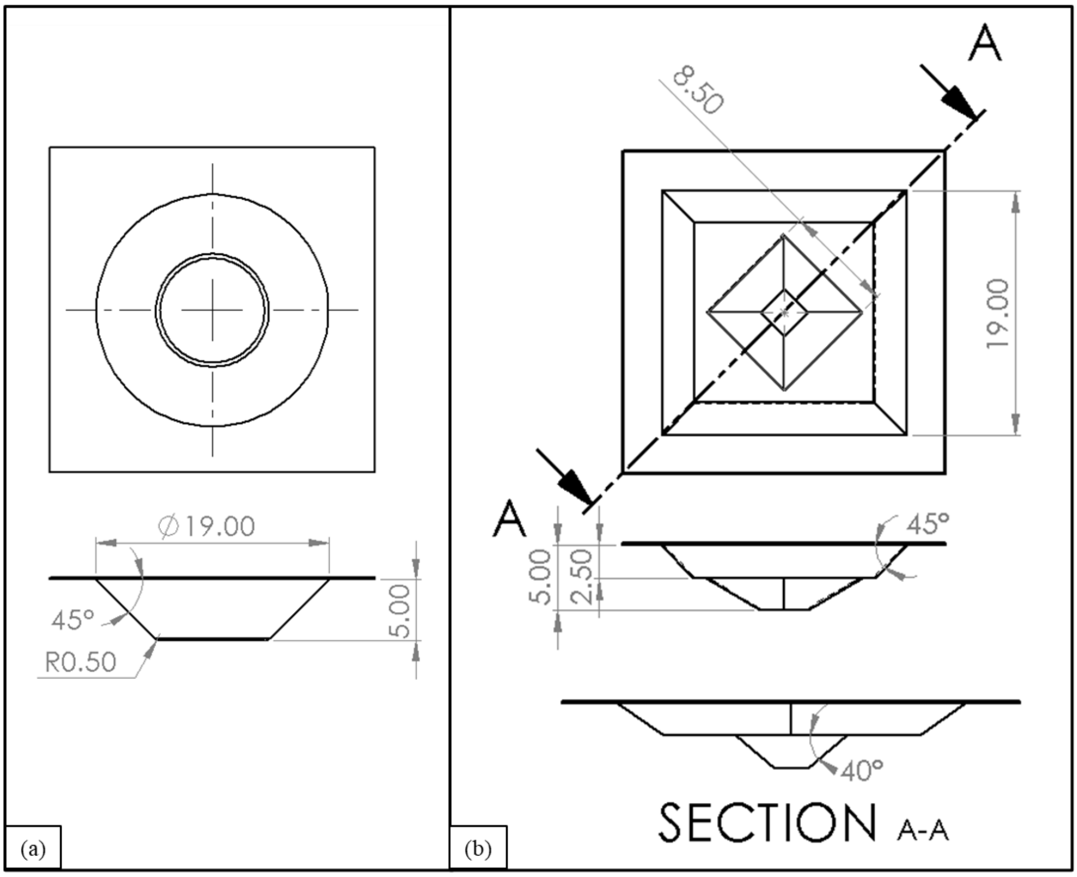

Figure 15 *CAD Drawings for (a) dome pyramid and (b) step pyramid. Units in mm.*

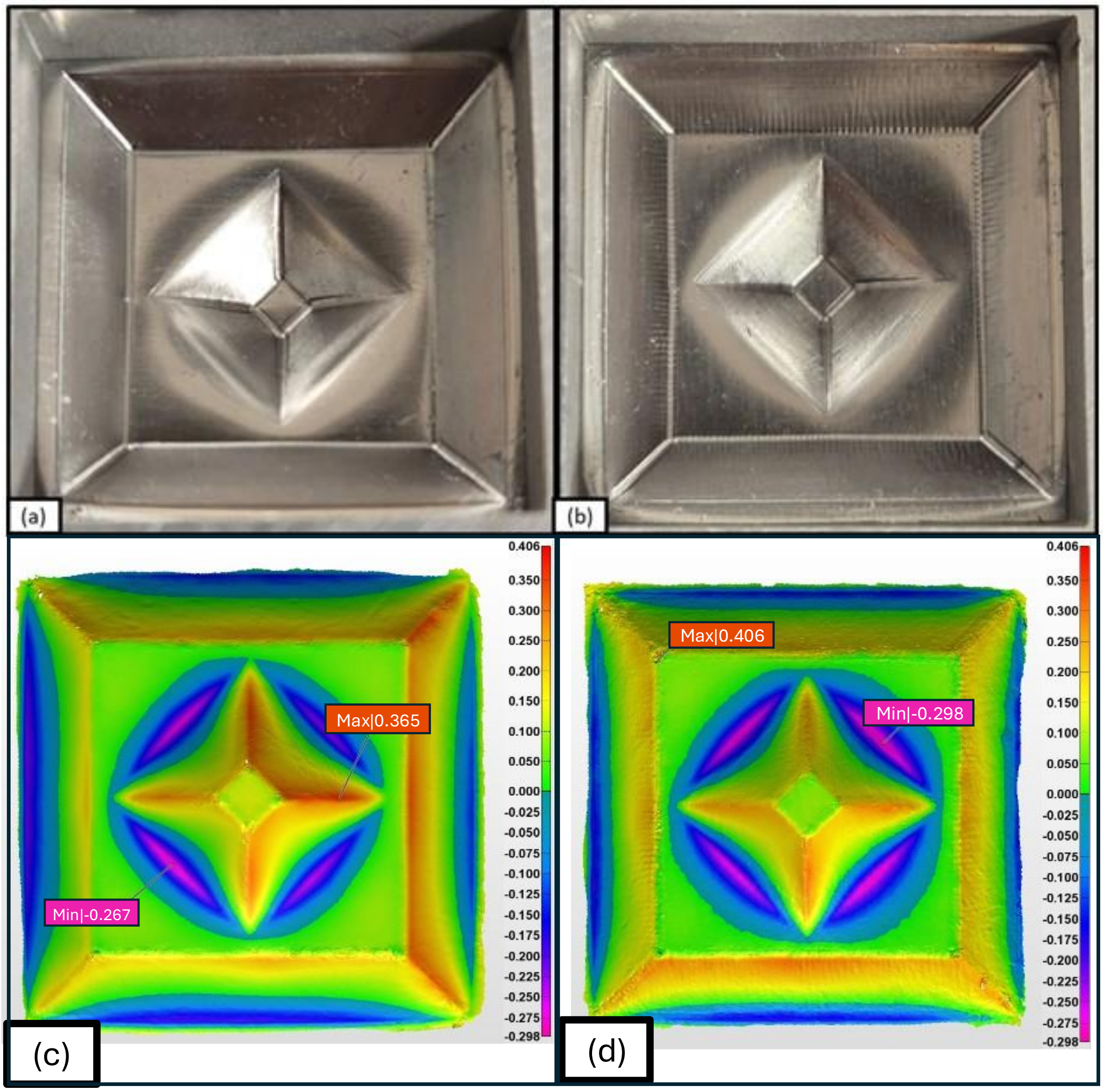

Figure 16 *Validation results on a hybrid pyramid shape using the best (a&c) and worst (b&d) forming parameters. Units in mm.*

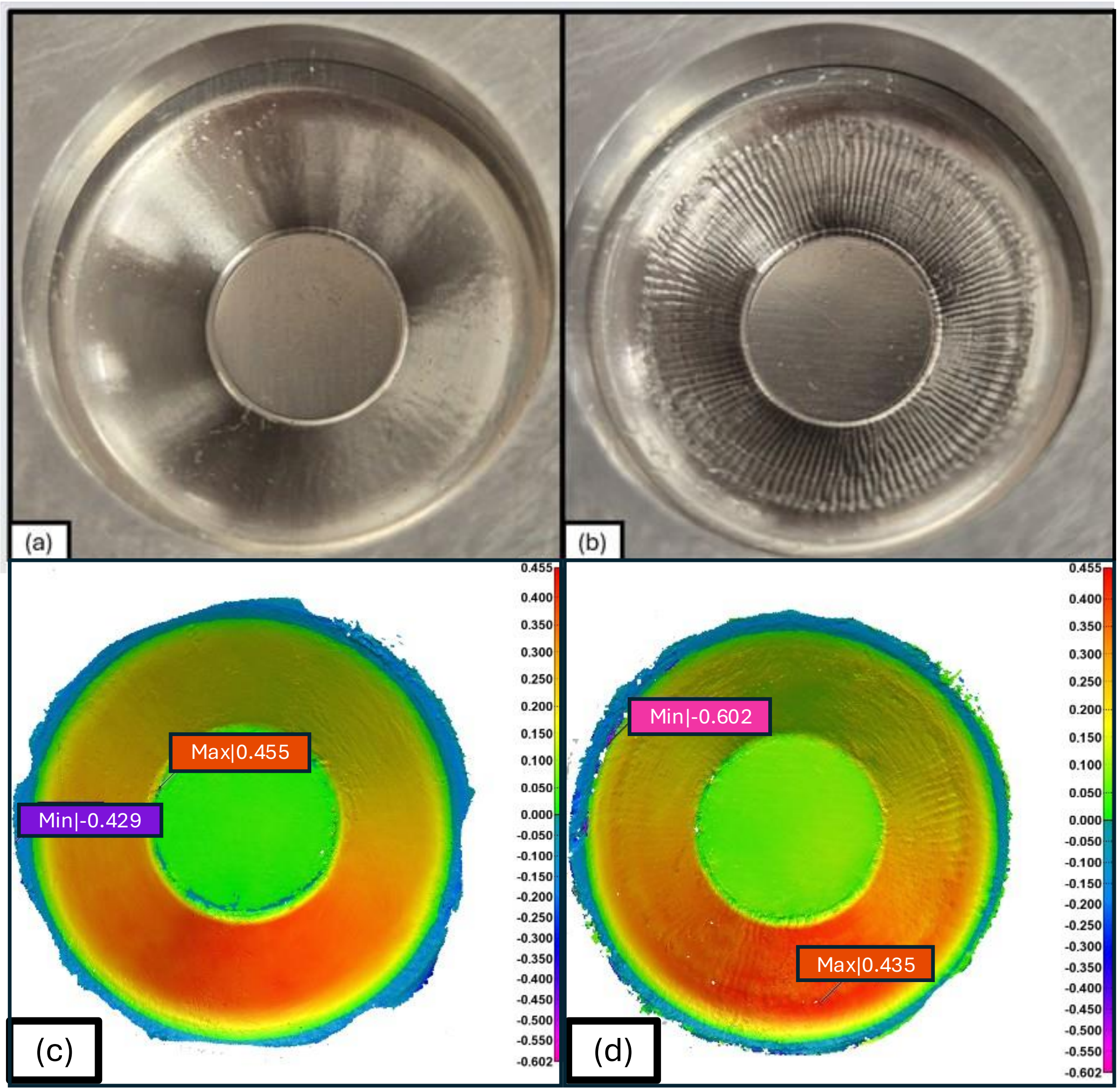

Figure 17 *Validation results for dome shape using the best (a&c) and worst (b&d) forming parameters. Units in mm.*

Additionally, the reduction of forming force with increasing spindle speed which was inferred early can also be visualised from **Figure 18**. Furthermore, **Figure 19** shows the change in MAD over the depth, which shows a correlation between elevated MAD and poor surface finish. Therefore, the use of MAD could be used for real-time detection of poor surface finish in micro-forming.

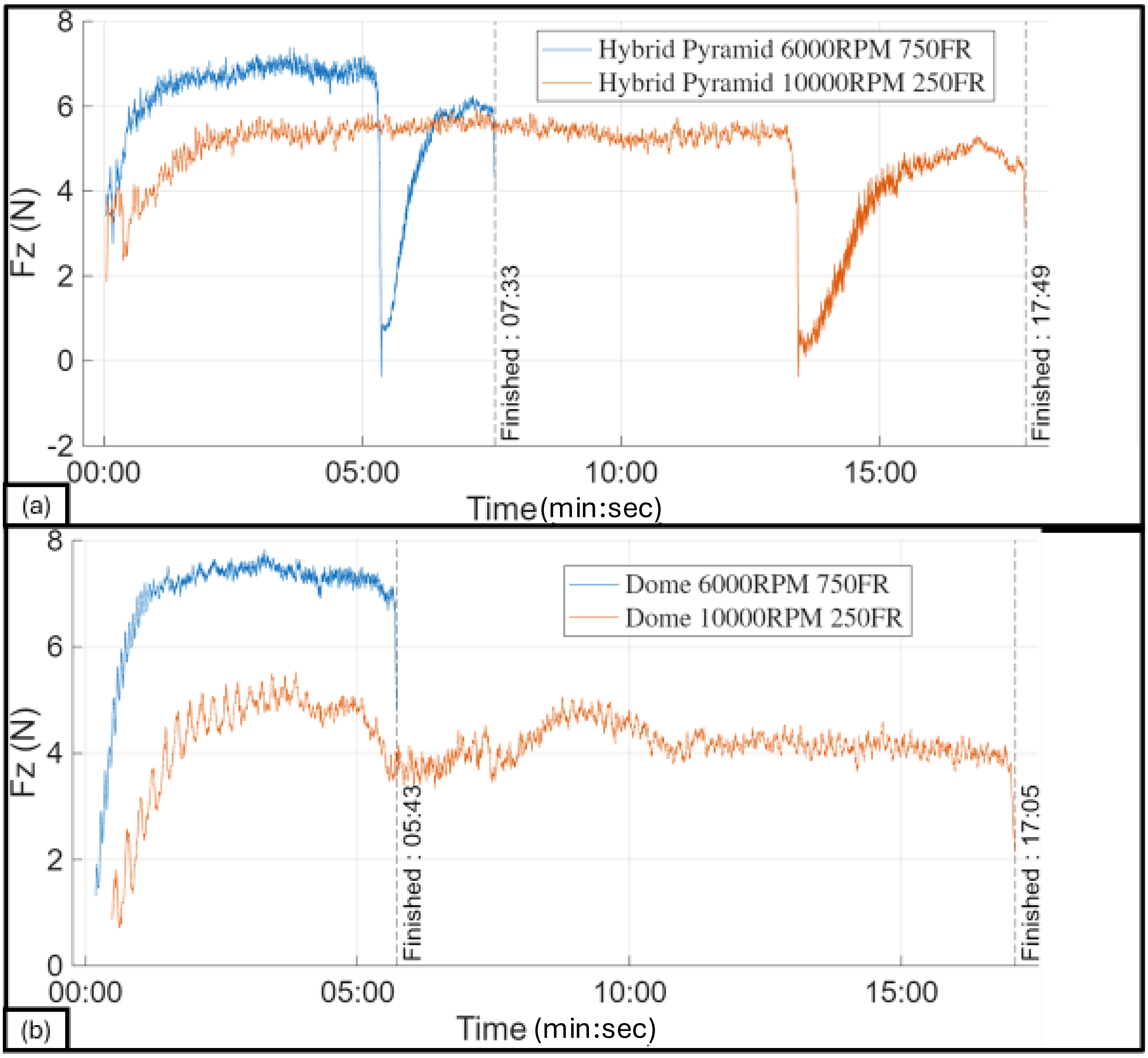

Figure 18 *Forming forces in Z-axis over time for (a) Hybrid Pyramid and (b) Dome shape. Vertical dashed lines indicate the finishing timing for the toolpath. Moving mean (1 second window) was applied to forming force to improve readability.*

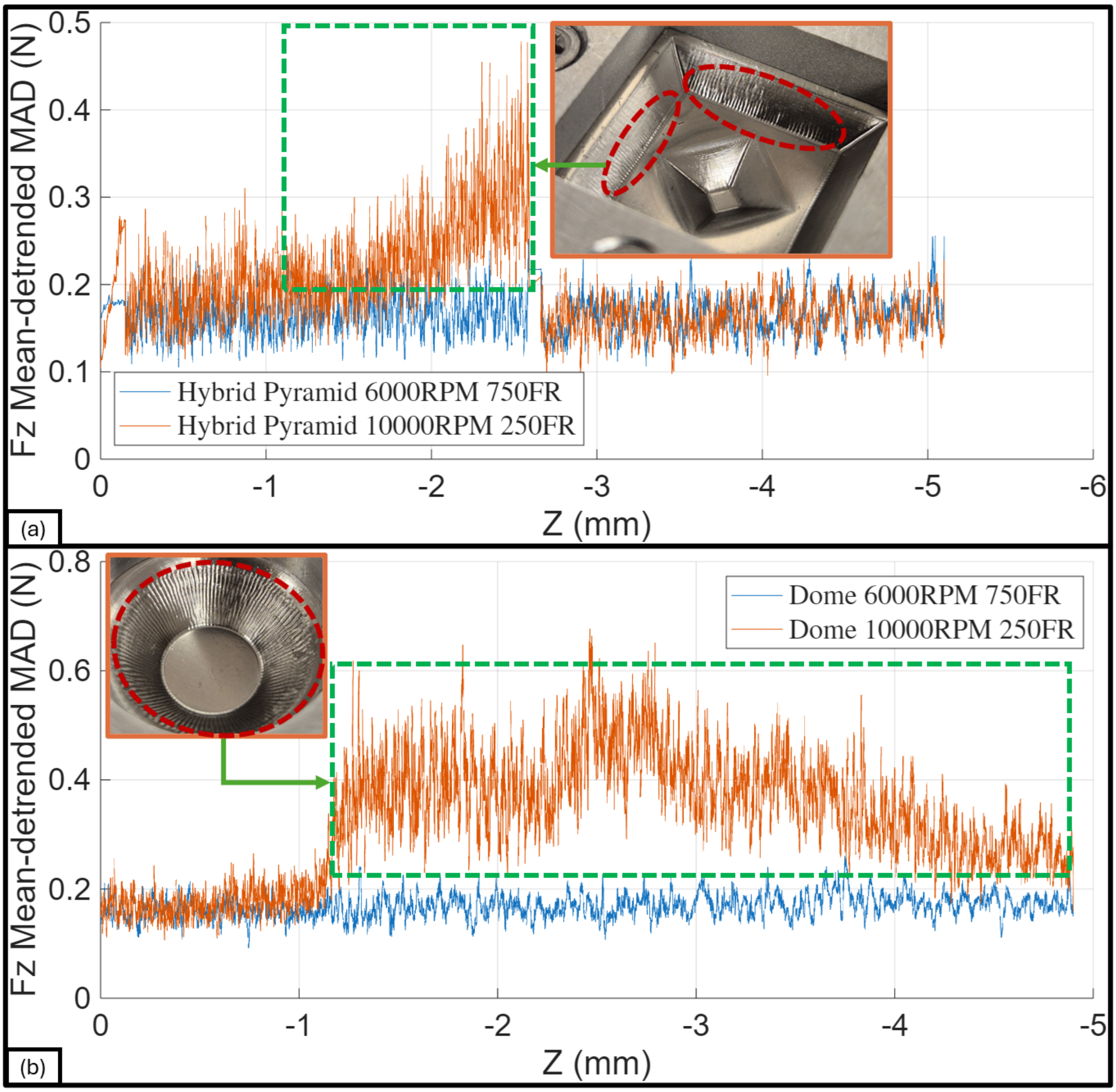

Figure 19 *Mean-detrended MAD for Fz for (a) Hybrid Pyramid and (b) Dome shape. The data was first subtracted by the moving mean (0.1 second window) prior to MAD (1 second window) calculation to minimise sudden trend changes that occur due to transition in hybrid shapes. Images of forming highlight areas of poor surface finish from 10,000 RPM and 250mm/min feed rate. A green dashed box highlights the regions in which the poor surface finish occurs.*

4. Conclusions

In conclusion, this study investigates the microformability of 304 stainless steel. Experimental investigations reveal that slender 1mm diameter ball-nose forming tools can have a detrimental effect on the surface finish. The study therefore focuses on the effects of two key process parameters, spindle speed and feed rate, on several performance metrics in $\mu SPIF$ of 304 stainless steel foils. Specifically, four sub-parameters were analysed: surface finish, mean forming force, force deviations, and geometric deviations.

The results showed a strong correlation between force deviations, measured through statistical analysis, and the observed and measured surface finish. The cyclic tool deflection manifested as periodic variations in forming forces, which were effectively captured by MAD measurements. This suggests that force deviation can be an effective metric for assessing the surface quality of formed parts, offering a practical and data-driven method for real-time process monitoring and optimization.

Additionally, the study found a clear relationship between the process parameters and mean forming forces. Higher feed rates were associated with increased forming forces, while faster spindle speeds led to a reduction in mean forces. Understanding these interactions between force and parameters can guide the selection of process settings to achieve desired force characteristics with increased productivity.

While the paper focused on finding the optimal set of parameters for improved surface finish, the converse could also have its applications. That is, the unique characteristics of the slender tool in $\mu SPIF$ with high RPM can readily produce the wrinkled texture surface during the forming process (**Figure 19**), which has implications in surface generation applications. Such applications have been previously demonstrated on the macro scale [20] but require the use of specialised forming tools. The surface texture generated in this paper was achieved using forming parameter selection, eliminating the need for specialised tooling.

Acknowledgements:

This research is supported by A*STAR under its Manufacturing of multi-material net-shape parts with heterogeneous properties (MMNH) Program (Grant reference No. M22K5a0045).

5. References

[1] J. G. R. Sereni, "Reference module in materials science and materials engineering," *Elsevier,* 2016.

[2] D. K. Bhatt, J. Rana, K. Shah and K. J. Patel, "Incremental sheet metal forming process: A review," *Int. J. Eng. Res. Technol,* vol. 4, p. 1–9, 2016.

[3] M. Popp, G. Rusu, S.-G. Racz and V. Oleksik, "Common defects of parts manufactured through single point incremental forming," in *MATEC Web of Conferences, EDP Sciences*, 2021.

[4] M. T. Mezher and B. Kovács, "An investigation of the impact of forming process parameters in single point incremental forming using experimental and numerical verification," *Periodica Polytechnica Mechanical Engineering,* vol. 66, no. 3, pp. 183-196, 2022.

[5] M. Pal, V. Pandya, C. K. Nirala and A. Agrawal, "Determining Critical Wall Angle in Micro-incremental Sheet Forming of SS316L Foils for Formability Assessment," *International Conference On Numerical Methods In Industrial Forming Processes, Springer International Publishing Cham,* p. 273–281, 2023.

[6] A. Jeevanantham, "Review on Micro Incremental Sheet Forming," *Journal of Chemical and Pharmaceutical Sciences 9,* 2016.

[7] P. Mahajan, J. Patil and S. Mishra, "Micro incremental forming of thin SS304 foils and its microstructural study," *IOP Conference Series: Materials Science and Engineering, IOP Publishing,* vol. 1284, p. 012045, 2023.

[8] R. G. Schreiber, L. S. S. Mondo, A. R. Teixeira, A. Daleffe and L. Schaeffer, "Predicting maximum force in SPIF for different materials," *Matéria, SciELO Brasil,* vol. 27, no. 4, 2022.

[9] S. Arshad, "SINGLE POINT INCREMENTAL FORMING: A study of Forming Parameters, Forming limits and Part accuracy of Aluminium 2024, 6061 and 7475 alloys," 2012.

[10] A. Bansal, B. Jiang and J. Ni, "Die-less fabrication of miniaturized parts through single point incremental micro-forming," *Journal of Manufacturing Processes, Elsevier,* vol. 43, p. 20–25, 2019.

[11] T. Muthusamy, A. Jeevanantham, R. Kishore and A. Rajeshkanan, "Formability and force analysis of steel foils in single point micro-incremental forming (SPMIF)," *Materials Today: Proceedings, Elsevier,* vol. 5, p. 12772–12781, 2018.

[12] A. A. Al-Bakri, Z. Sajuri, A. K. Ariffin, M. A. Razzaq and M. S. Fafmin, "Tensile and fracture behaviour of very thin 304 stainless steel sheet," *Jurnal Teknologi (Sciences & Engineering),* vol. 78, no. 6-9, 2016.

[13] D. L. W. Wen, H. G. Soon and A. S. Kumar, "Micro-milling digital twin for real-time tool condition monitoring," *Manufacturing Letters, Elsevier,* vol. 41, p. 1231–1236, 2024.

[14] D. Nasulea and G. Oancea, "Research on manufacturing of pyramidal frustum parts using single point incremental forming process," *IOP Conference Series: Materials Science and Engineering, IOP Publishing,* vol. 564, p. 012019, 2019.

[15] Z. Cheng, Y. Li, C. Xu, Y. Liu, S. Ghafoor and F. Li, "Incremental sheet forming towards biomedical implants: A review," *Journal of Materials Research and Technology, Elsevier,* vol. 9, no. 4, p. 7225–7251, 2020.

[16] S. M. Najm, I. Paniti, T. Trzepieciński, S. A. Nama, Z. J. Viharos and A. Jacso, "Parametric effects of single point incremental forming on hardness of AA1100 aluminium alloy sheets," *MDPI,* vol. 14, no. 23, p. 7263, 2021.

[17] W. Tillmann, D. Stangier, A. Meijer, E. Krebs, A. Ott, T. Platt, N. Lopes Dias, L. Hagen and D. Biermann, “Adapting the Surface Integrity of High-Speed Steel Tools for Sheet-Bulk Metal Forming,” vol. 6, no. 2, 2022.

[18] A. Petek, K. Kuzman and J. Kopaè, “Deformations and forces analysis of single point incremental sheet metal forming,” *Archives of Materials Science and Engineering,* vol. 35, no. 2, 2009.

[19] G. Mandaloi, A. Nagargoje, A. K. Gupta, G. Banerjee, H. Y. Shahare and P. Tandon, “A Comprehensive Review on Experimental Conditions, Strategies, Performance, and Applications of Incremental Forming for Deformation Machining,” *Journal of Manufacturing Science and Engineering, ASME International,* vol. 144, no. 11, 2022.

[20] P. Kang, S. Huang, B. Beckle, E. S. Cifuentes, L. Feng, K.-C. Park, K. Ehmann and J. Cao, “Toolmarks-Driven Surface Texture for Coating Attachment With Drag Reduction and Anti-Biofouling Performance,” *International Manufacturing Science and Engineering Conference, American Society of Mechanical Engineers,* vol. 87240, p. V002T06A023, 2023.